# Curvature Modification of Block Copolymer Microdomains Using Blends of Block Copolymers with Hydrogen Bonding Interactions

**ARTICLE** *in* MACROMOLECULES · NOVEMBER 2012

Impact Factor: 5.8 · DOI: 10.1021/ma301402n



**4 AUTHORS**, INCLUDING:

Victor Alexandrovich Pryamitsyn
Northwestern University
**102** PUBLICATIONS **2,490** CITATIONS
SEE PROFILE

Sung Hyun Han
Samsung Advanced Institute of Technology
**15** PUBLICATIONS **185** CITATIONS
SEE PROFILE

Macromolecules

Article

pubs.acs.org/Macromolecules

# Curvature Modification of Block Copolymer Microdomains Using Blends of Block Copolymers with Hydrogen Bonding Interactions

Victor Pryamitsyn,[†] Sung Hyun Han,[‡] Jin Kon Kim,[‡] and Venkat Ganesan[†,*]

[†]Department of Chemical Engineering, University of Texas at Austin, Austin, Texas 78712, United States

[‡]National Creative Research Center for Block Copolymer Self-Assembly, Department of Chemical Engineering, Pohang University of Science and Technology, Kyungbuk 790-784, Korea

Supporting Information

**ABSTRACT:** We present a strong stretching theory model for microphase segregation of AB + AC block copolymer blends in which the B and C segments possess strongly attractive (hydrogen bonding) interactions. In microphase separated morphologies, we demonstrate that the attraction between the B and the C segments causes a bending force toward the A layers. Such bending forces may induce transitions from lamellar and A-majority cylindrical morphologies in the pure component systems to "inverted" cylindrical and spherical morphologies in blends in which the B and C segments constitute the matrix phase. Similar driving forces may also drive transitions from A-majority spherical phases in pure component systems to highly asymmetric lamellar morphologies in blends. The predictions of our model are in excellent agreement with the trends observed in recent experimental results.

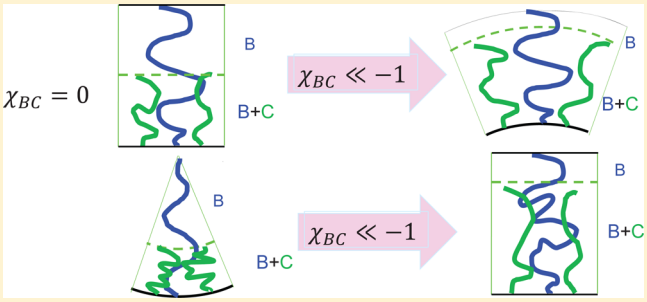


## I. INTRODUCTION

Recently, the self-assembly characteristics of block copolymers has emerged as an active topic of interest for a variety of applications.[1−10] A large fraction of the work in this context has focused on the simplest case of AB diblock copolymers, which consist of segments of type A monomers covalently bonded to segments of type B monomers. In such systems, the morphology arising from self-assembly is controlled by the composition of the block copolymer (the average volume fraction of the A segments), $f$, the Flory−Huggins interaction parameter between the A and B segments, $\chi$, and the degree of polymerization of the polymer chain $N$.[11,12] By varying $f$ and $\chi N$, different morphologies such as lamellae, hexagonally packed (HEX) cylinders, body-centered-cubic (BCC) spheres and bicontinuous gyroid phases have been obtained.[11−13] Since the size, shape, and periodicity of the resulting self-assembly patterns can be tuned by varying the molecular weight and compositions, block copolymers (BCPs) have received significant attention in the context of applications such as nanostructured membranes, templates for nanoparticle synthesis, photonic crystals, and lithography for high-density information storage media.[1−5,8,10,14−16]

Despite the significant progress achieved in understanding and controlling block copolymer self-assembly, there still remain some outstanding challenges. For instance, the morphology of the periodic patterns are strongly correlated to the composition of the copolymer. Indeed, for a diblock copolymer, lamellar patterns result when the volume fractions of the blocks are comparable to one another.[11,12] When the composition of the block copolymer is asymmetric (i.e., the volume fraction of one of the blocks becomes substantially different from the other), cylindrical, gyroid or spherical patterns result. Unfortunately, these considerations limit the geometrical characteristics achievable in the self-assembly patterns of block copolymers.[11,12,17,18] For instance, asymmetric line patterns, i.e., lamellar morphologies in which one of the microdomains is significantly larger than the other, cannot be achieved using conventional diblock copolymer self-assembly. Likewise, spherical and cylindrical self-assembly patterns in which the enclosed phase possesses a volume comparable or larger than the matrix, cannot be fabricated straightforwardly through block copolymer self-assembly.

Since the morphologies achievable by a single component block copolymer system are limited by their average volume fractions and temperature, a potential alternative strategy to address the above challenges would be to use blends of diblock copolymers. Motivated by such considerations, several experimental studies have examined the phase behavior of binary blends of diblock copolymers which are chemically identical but differing in their compositions and/or molecular weights.[19−33] While intriguing morphological transitions have been demonstrated in such contexts,[19−33] achieving highly asymmetric lamellar patterns and/or high internal volume spherical or cylindrical phases is not tractable even within such systems.

Recently, we demonstrated that by using binary blends of A−B and A−C diblock copolymers of different molecular weights in which there are specific hydrogen (H−) bonding interactions

**Received:** July 6, 2012
**Revised:** September 20, 2012
**Published:** October 18, 2012

between the B and C blocks,[34,35] we can overcome the inherent curvature limitations of single component and binary blends of diblock copolymers. Specifically, we considered binary blends consisting of high molecular weight polystyrene-*block*-poly(2-vinylpyridine) copolymer (PS-*b*-P2VP, denoted AB copolymer in this article) and low molecular weight polystyrene-*block*-poly(4-hydroxystyrene) copolymer (PS-*b*-PHS, denoted $A_sC$ in this article). Such systems exhibit the property that the PS (A and $A_s$) blocks are immiscible with both P2VP (B) and PHS (C) blocks, however, the P2VP (B) and PHS (C) blocks exhibit strongly attractive hydrogen bonding interactions with one another. We effected two classes of experiments:

- In one set of experiments,[35] we used a blend of asymmetric ($f_A$ and $f_{A_s} \simeq 0.8$) PS-*b*-P2VP and PS-*b*-PHS block copolymers. Each of the individual block copolymers displayed spherical microdomains over the entire range of experimental temperature conditions. However, by modulating the amount of PS-*b*-PHS added to the blend, we demonstrated that the spherical microdomains can be transformed to HEX cylinders and to lamellar morphologies. Interestingly, since the width ratio of the lamellar microdomains are approximately set by $f_A$ (for $f_A = f_{A_s}$, the width ratio is approximately $f_A/(1 - f_A)$), we were able to achieve highly asymmetric lamellar microdomains. We also demonstrated that by using appropriate techniques, such blends can be made to retain their morphologies even in thin film conditions, which pointed to the potential of such structures in the context of next-generation block copolymer lithography.
- In another series of experiments,[34] we employed a blend of almost symmetric ($f \simeq 0.5$) PS-*b*-P2VP and PS-*b*-PHS block copolymers. The pure component block copolymers displayed lamellar microdomains over the entire range of experimental temperature conditions. However, by modulating the amount of PS-*b*-PHS added to the blend, we demonstrated that the lamellar microdomains can be transformed to HEX cylinders and BCC spherical morphologies. For the case of a relatively higher molecular weight (MW) PS-*b*-PHS (but still lower than the MW of PS-*b*-P2VP), only HEX cylinders were observed even at large amounts of PS-*b*-PHS in the blend. In contrast, when a relatively low molecular weight PS-*b*-PHS was blended with PS-*b*-P2VP, we observed that the lamellar phase of PS-*b*-P2VP transitions to HEX cylinders at small concentrations of PS-*b*-PHS, whereas, with further addition of PS-*b*-PHS copolymers, BCC spherical phases resulted. Since the two components of the blend are symmetric in their compositions, the cylindrical and spherical phases formed in the system were such that the core (i.e., the regions inside the sphere or the cylinder) had the same volume as the "matrix" phase (i.e., the phase outside the sphere or cylinder), and hence, the radii of the interior phase constituted a substantial fraction of the resulting unit cell of the morphology. To contrast, we note that the cylindrical or spherical phases which are formed in monodisperse, single component AB diblock copolymer systems are typically asymmetric in the volumes occupied, and hence the radii of the interior phases are comparatively much smaller relative to the unit cell dimensions.

Overall, the above experimental results conclusively demonstrated that the use of a binary blend of block copolymers with H-bonding interactions between the blocks may provide a strategy to modify the curvature of the underlying block copolymer microdomains, and thereby create "symmetric" cylindrical/spherical morphologies and "asymmetric" lamellar patterns. However, a number of outstanding questions still remain in an effort to translate the experimental observations into a general strategy. For instance, the mechanisms underlying the curvature transformations were only briefly discussed in our experimental articles,[34,35] and the details of the quantitative model which embodies the mechanisms underlying such phase transformations were not elaborated. Moreover, the dependence of the morphological transformations upon parameters such as the A−B, A−C, and B−C interactions, the ratio of the molecular weights of the A−B and A−C copolymers and their blending compositions was also not delineated. Also, we did not explore the limits of block copolymer compositions to which such curvature modification ideas can be generalized.

In light of the vast parameter space that accompanies binary blends of block copolymers, theoretical calculations and computer simulations are likely to prove more useful to address the above issues. Indeed, in the related system of blends of chemically identical diblock copolymers, theories and simulations have shed important insights into the origins of their complex phase behavior. For instance, using polymer self-consistent field theory (SCFT),[36,37] Shi, Noolandi and co-workers,[38−41] Matsen,[42,43] and others[44,45] have constructed phase diagrams of binary blends of diblock copolymers and identified the influence of the different physicochemical parameters. In a series of articles, Birhstein and co-workers examined the phase behavior of binary blends of diblock copolymers using strong segregation theory.[46−51] Their predictions were in very good agreement with the experimental results of Hashimoto and co-workers[23−25]

Motivated by the useful insights furnished by the above theoretical studies, in this work we present a strong stretching theory (SST) based model for the phase behavior of AB + AC blends with strong hydrogen bonding interactions between B and C components. Using such a model, we explore the morphological phase behavior of AB + AC blends as a function of different physicochemical parameters. The development of our theory is general, and in fact can be straightforwardly extended to treat other cases of AB + CD blends[52−55] in which the pairs A, D and B, C have favorable interactions, but the other pairs have repulsive interactions. However, in this article, we focus on parametric conditions which are close to those explored in our own experiments and restrict our attention only to mixtures of AB + $A_sC$ diblock copolymers. We delineate the physics underlying the experimental results and explore the parametric conditions requisite to achieve asymmetric lamellar patterns and high internal volume curved phases.

The rest of the article is arranged as follows: In section IIA, we present a hypothesis for the mechanisms underlying the experimentally observed morphological phase transformations. Subsequently, in section IIB, we present the mathematical formulation of the SST model which forms the basis of our predictions. In section III, we present the numerical results based on our SST model. In section IIIA, we present a few representative results for the case of a binary blend of AB diblock copolymers (with differing compositions) and compare it with the predictions of other theories and calculations. Subsequently, in section IIIB, we present results for mixtures of AB + $A_sC$ diblock copolymers. We conclude with a brief summary and outlook for future work.

## II. STRONG STRETCHING THEORY

**A. Mechanisms Underlying the Phase Transformations in AB + $A_sC$ Blends.** Prior to a discussion of the mechanisms underlying the phase transformations noted in our experiments, we first present some details of the parameters which characterize the experiments motivating the present work.[34,35] As mentioned in the introduction, the experiments considered a blend of PS-*b*-P2VP and PS-*b*-PHS diblock copolymers. We denote the total number of segments in PS-*b*-P2VP as $N$ and the number of segments in PS-*b*-PHS as $N_s$. In the experiments, $N \simeq 1100$, and $N > N_s$ such that the ratio $\alpha = N_s/N$ was varied (approximately) in the range 0.25−0.5 in the first series of experiments,[35] and in the range 0.08−0.5 in the second series of experiments.[34] The Flory−Huggins interactions parameter for PS and P2VP is of the order 0.1 at the experimental range of temperatures. In contrast, PS and PHS are extremely incompatible polymers and possess a Flory−Huggins interaction parameter of the order of 0.6.[56−59] Hence, even the smallest molecular weight of PS-*b*-PHS probed in the experiments (∼8000) possessed a well-segregated morphology. Moreover, the P2VP and PHS segments exhibit strongly attractive H-bonding interactions.[60,61]

We note that in the context of second set of experiments,[34] we complemented the observations with the results of polymer self-consistent field theory (SCFT) to explain the transformation of binary blends of symmetric block copolymers from lamellar patterns to cylindrical and spherical morphologies. Because of numerical limitations, we could only probe much weaker interaction parameters (we set $\chi_{AB}N_{AB} = 20.0$ and $\chi_{AC}N_{AB} = 120.0$) compared to experimental conditions. On the basis of the numerical results, we suggested that the phase transformations noted in the experiments were primarily driven by a dissolution of the short chain A−C copolymers in the B phase.[39,62] Such a dissolution was argued to occur as a consequence of the attractive H-bonding interactions between the B and C copolymers which could overcome the unfavorable A−B interactions accompanying the solubilization of AC copolymers. We suggested that such dissolution leads to an increase in the "effective volume fraction" of B segments, and thereby triggers a transition to curved phases in which the B and C segments constitute the matrix of the morphology.

In the present work, we revise our above proposal to suggest that the dissolution of A−C copolymers into the B phase is likely to constitute only one of the contributions to the mechanisms underlying the phase transformations noted in our experiments (cf. Figure 1). We suggest that such a contribution

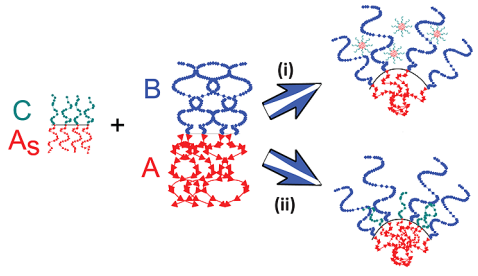


**Figure 1.** Two possible mechanisms to explain the influence of $A_sC$ chains on the morphologies of AB diblock copolymers. (i) The $A_sC$ copolymers dissolve in the B phase and increase the effective volume fraction of the B component; (ii) The $A_sC$ copolymers segregate to the AB interface and modify the curvature through hydrogen bonding interactions.

is likely to be relevant only under the conditions in which $\chi_{BC}$ is large and negative, $\chi_{AB}$ is not too large, and if the A segments constitute the minority component in the AC copolymers. However, for strong incompatibility parameters $\chi_{AB}$, $\chi_{AC}$ (which fall in the regime of the experimental conditions, but were however beyond the regimes probed in our SCFT model[34]) and/or for the cases of symmetric and highly asymmetric AC copolymers with a majority A component, the dissolution of AC block copolymers in the B phase is very unlikely. Instead, the AC copolymers are more likely to remain at the interface between the A and B segments.[62] Indeed, in the first set of experiments,[35] the ratio of the lamellar widths of the asymmetric lamella was found to be consistent with what one would expect if the AC copolymers were located at the interface between A and B + C phases. On the basis of such considerations, in the present work, we suggest an alternative mechanism which relies on the interfacial localization of the AC copolymers to explain our experimental results.

To explain the physical basis of the morphological changes noted in the experiments, we envision a scenario in which we start from a pure A−B block copolymer system that is either arranged in lamellar (symmetric) or curved (for specificity, we assume that these are spherical morphologies) morphologies (see Figure 2). Moreover, we assume that the added AC

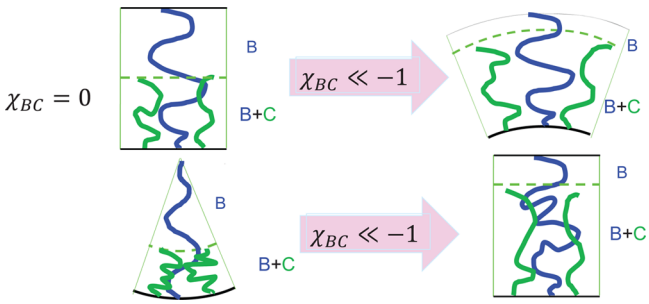


**Figure 2.** Schematic of the proposed mechanism for transformation of lamellar morphologies to convex morphologies and concave morphologies to lamellar phases.

copolymers are located at the interface between A and B segments. With increasing amount of added A−C chains, the H-bonding interactions between B and C segments favors the enhanced mixing of B and C segments. Such tendencies force the (smaller) C chains to stretch and the (longer) B chains to compress. Since morphologies which are convex toward the B and C components facilitate easier mixing between the B and C segments without a corresponding increase in stretching energy, spherical morphologies transform to less concave cylindrical phases and subsequently to the nonconcave lamellar morphologies. In a similar manner, for an initially symmetric system which exists in the lamellar morphology, addition of AC chains leads to curved morphologies (spheres and cylinders) which are bent outward toward B and C chains.

**B. SST Model.** In this section, we translate the hypothesis presented in the preceding section into a mathematical model based on the strong stretching theory (SST).[63−65] A number of previous studies have successfully used SST based models to characterize the density profiles of polymer brushes,[64,66,67] phase behavior of multicomponent copolymers,[68−72] equilibrium organization in block copolymer−nanoparticle mixtures[73,74] etc. While SST models have been shown to be quantitatively accurate only at very high degrees of segregation, nevertheless, such models are useful due to their analytical simplicity and their ability to capture the qualitative trends of phase behavior. It is within the latter spirit


dx.doi.org/10.1021/ma301402n | Macromolecules 2012, 45, 8729−8742

we undertake the development of the SST model for the phase behavior of AB + AC blends.

In this section, we develop a thermodynamic model for the morphological characteristics of AB + $A_s$C blends. We consider the energy contributions arising from chain stretching, the favorable enthalpic interactions between B and C segments, and the interfacial tension costs between the A and B + C phase. As candidate morphologies, we consider the homogeneous phase, lamellar phases, and both convex and concave (with respect to A segments) cylindrical and spherical phases (cf. Figure 3). We

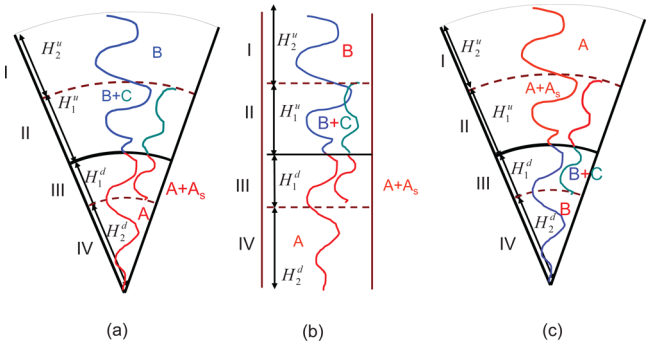


**Figure 3.** Schematic of the different morphologies considered for our analysis and the notations used in the main text: (a) cylindrical or spherical morphologies with an A core; (b) lamellar morphologies; (c) cylindrical or spherical morphologies with a BC core. I, II, III and IV and denote the different regions which are considered individually in the main text. $H_2^u$,$H_1^u$,$H_1^d$, and $H_2^d$ denote the respective thicknesses of the regions I–IV.

minimize the net free energy to deduce the optimal period for a specified structure and identify the structure which possesses the lowest free energy among the different morphologies.[46−51,63] We note that consideration of other possible self-assembly morphologies, such as gyroid phases may modify the results presented in the following section. However, analysis of such phases occurs at the expense of considerable complexity, and hence we eschew such an effort in this work.

For our model, we assume that the A, B and C portions of the polymer are all flexible polymer chains and that the segments possess identical monomeric volumes denoted $b^3 = \rho_0^{-1}$, where $b$ denotes the Kuhn segment and $\rho_0$ is the average density of polymer blend. We use $N_A$ and $N_B$ to denote the number of A and B segments respectively in the AB chains ($N = N_A + N_B$), and $N_{sA}$ and $N_C$ to denote the number of A and C segments in the AC chains ($N_s = N_{sA} + N_C$). Moreover, the ratio of molecular weights of the AB and AC chains is denoted as $\alpha = N_s/N$ and without loss of generality assume that $\alpha < 1$. The unperturbed radius of gyration of the AB chains is denoted as $R_g = b(N/6)^{1/2}$. The enthalpic interactions are characterized by Flory interaction parameters between A, B, and C segments and are denoted as $\chi_{AB}$, $\chi_{AC}$, and $\chi_{BC}$ respectively. Note that we are considering blends in which the B and C segments exhibit strong associative interactions arising from H-bonding forces. While different approaches exist to model H-bonding interactions,[75,76] we use the simplest of these approaches by choosing to represent the H-bonding interactions through a Flory–Huggins like interaction parameter $\chi_{BC}$ which is negative. The other interaction parameters are chosen such that $\chi_{AB}$, $\chi_{AC} > 0$. The compositions of AB and short AC chains are defined by the parameters: $f = N_A/N$ and $f_s = N_{sA}/N_s$. The amount of AC chains in the blend is quantified by the volume or the weight fraction of AC chains, which is denoted as $w$. The number of AC chains per AB chain is denoted as $n_s$, and is related to $w$ and $\alpha$ through

$$n_s = \frac{w}{\alpha(1-w)} \tag{1}$$

All free energies below are expressed on the basis of per AB chain and are in units of $k_BT$.

*Free Energy of Homogeneous Phases.* The free energy of a *homogeneous* blend of AB and AC chains (denoted as "disordered" morphology in phase diagrams), denoted as $F_{iso}$, is given by

$$\frac{F_{iso}}{N} = (1-f)[f(1-w) + f_s w]\chi_{AB} + \frac{w}{1-w}(1-f_s) \times [f(1-w) + f_s w]\chi_{AC} + w(1-f)(1-f_s)\chi_{BC} \tag{2}$$

*Free Energy of the Microdomain Structures.* Figure 3 presents a pictorial representation of the notations used in our model for the construction of free energies of segregated phases. We consider the following candidate structures for microphase separated morphologies: (i) lamellar phases (Figure 3b); (ii) cylindrical phases containing A chains in the core (Figure 3a); (iii) cylindrical phases containing B and C chains in the core (referred to henceforth as BC core) (Figure 3c); (iv) spherical phases containing A chains in the core (Figure 3a); (v) spherical phases with BC core (Figure 3c).

To identify the free energies of the microphase separated morphologies, we divide the morphologies into four zones: Region I constitutes the outermost region of the structure, whose thickness is denoted as $H_2^u$. This region is populated by A (B) segments for a BC (A) core configuration. Region IV constitutes the innermost region of the structure, whose thickness is denoted as $H_2^d$. This region is populated by B (A) segments for a BC (A) core configuration. We use the symbol $N_2^u$ and $N_2^d$ to denote the number of segments of the AB chain which lies in the regions I and IV respectively. Region II constitutes the interior region in the corona and consists of a mixture A and $A_s$ (B and C) segments for a BC (A) core configuration. The thickness of region II is denoted as $H_1^u$ and the number of segments of the AB copolymer which are located in this region is denoted as $N_1^u$. Region III constitutes the interior region in the core of the structure and consists of a mixture B and C (A and $A_s$) segments for a BC (A) core configuration. The thickness of region III is denoted as $H_1^d$ and the number of segments of the AB copolymer which are present in this region is denoted as $N_1^d$. We have the following relationships between $N_1^u$ $N_2^u$ $N_1^d$ and $N_2^d$:

$$N_1^u + N_2^u = \begin{cases} Nf & \text{BC core} \\ N(1-f) & \text{A core} \end{cases} \tag{3}$$

and

$$N_1^d + N_2^d = \begin{cases} N(1-f) & \text{BC core} \\ Nf & \text{A core} \end{cases} \tag{4}$$

The symbol $\sigma$ (in units of $b^{-2}$) is used to denote the grafting density of AB chains. In other words, $\sigma b^{-2}$ represents the number of AB chains per unit area of the interface. The constraints of incompressibility allow us to relate the thickness $H_1^u$, $H_2^u$, $H_1^d$, and $H_1^d$ to $N_1^u$, $N_2^u$, $N_1^d$, and $N_2^d$


dx.doi.org/10.1021/ma301402n | Macromolecules 2012, 45, 8729–8742

in the different geometries. For instance, for the lamellar phases we have

$$H_2^u = N_2^u \sigma b \tag{5}$$

$$H_2^d = N_2^d \sigma b \tag{6}$$

$$H_1^u = \begin{cases} (N_1^u + n_s \alpha N f_s)\sigma b & \text{BC core} \\ [(N_1^u + n_s \alpha N (1 - f_s)]\sigma b & \text{A core} \end{cases} \tag{7}$$

$$H_1^d = \begin{cases} [N_1^d + n_s \alpha N (1 - f_s)]\sigma b & \text{BC core} \\ (N_1^d + n_s \alpha N f_s)\sigma b & \text{A core} \end{cases} \tag{8}$$

Comparable expressions for the cylindrical and spherical geometries can be derived by using straightforward geometric arguments. To maintain brevity, we do not display the corresponding expressions for the other geometries.

The free energy of the microphase separated morphologies can then be obtained by considering each of the four regions independently and identifying the different energetic contributions arising from therein:

*Region I.* In region I, the free energy contributions (denoted as $F_I$) arise only from the elastic stretching energy costs of the A (or B) segments. The effective grafting density of the chains in this region is denoted $\sigma_+$, where

$$\sigma_+ = \sigma \left(1 + \frac{H_1^{(u)}}{R}\right)^{1-D} \tag{9}$$

in which $D = 1$ for lamellae, $D = 2$ for cylinders and $D = 3$ for spheres. In the above, $R = H_1^d + H_2^d$ denotes the radius of the core of the morphology. The elastic free energy for such a convex brush of monodisperse chains (grafted on a surface of radius $R + H_1^u$) was calculated by Semenov as[63]

$$F_I = \begin{cases} \frac{\pi^2}{8} N_2^u b^2 \sigma^2 & \text{flat brush} \\ \frac{3}{4} R b \sigma_+ \log\left(\frac{2 b N_2^u \sigma_+}{R + H_1^u} + 1\right) & \text{cylindrical brush} \\ \frac{3}{2} R b \sigma_+ \left(1 - \left(\frac{3 N_2^u b \sigma_+}{R + H_1^u} + 1\right)^{-1/3}\right) & \text{spherical brush} \end{cases} \tag{10}$$

*Region IV.* The free energy contribution in this region, denoted $F_{IV}$, also arises only from the elastic stretching energy costs of the A or B segments. The effective grafting density of the chains in this region is denoted $\sigma_-$, where

$$\sigma_- = \sigma \left(1 - \frac{H_1^{(d)}}{R}\right)^{1-D} \tag{11}$$

and the effective curvature of the brush is $R - H_1^d$. The elastic free energy for such a concave brush was calculated by Semenov and is given as:[63]

$$F_{IV} = \begin{cases} \frac{\pi^2}{8} N_2^d b^2 \sigma^2 & \text{flat brush} \\ \frac{\pi^2}{4} N_2^d b^2 \sigma_-^2 & \text{cylindrical brush} \\ \frac{27}{80} \pi^2 N_2^d b^2 \sigma_-^2 & \text{spherical brush} \end{cases} \tag{12}$$

*Regions II and III.* Regions II and III are characterized by three energy contributions: (i) the stretching energies $F^{el}$ of bidisperse brushes made of a mixture of B, C chains and A, $A_s$ chains; (ii) the enthalpic contribution $F^{en}$ arising from the mixing of B and C segments; (iii) the interfacial tension cost, $F^{int}$, for the interface between regions II and III.

To address the stretching energy contributions, we need an expression for the elastic energy of a brush which consists of a binary mixture of chemically distinct chains (to model the region containing B and C segments) possessing different MWs, in both convex and concave configurations of lamellar, cylindrical and spherical geometries.[46−50,66,77] A strong stretching approximation for bidisperse brushes of chemically identical chains was developed by Lyatskaya, Zhulina, and Birshtein for the cases of flat and cylindrical brushes.[46−50] Unfortunately, a direct extension of their formalism to spherical geometries becomes prohibitively complicated. Moreover, the method suggested by Birshtein and co-workers[46−50] applies only for bidisperse brushes of polymer chains of the same chemical identity and therefore, in our case would not apply to the regions occupied by B and C segments.

To develop a tractable analytical model for the elastic energy contribution of a bidisperse brush in the different situations considered in this article, we use an *ad-hoc* assumption that within the regions II and III, the local stretching of the two kinds of chains which constitute the brush are proportional to each other. Moreover, we assume that the proportionality between the local stretching of the chains is independent of the location in the plane normal to the grafting surface. Such an assumption is inspired by the deGennes−Alexander[78,79] approximation for a flat brush but is however not rigorously justifiable for curved geometries. However, in the later sections, we demonstrate that the predictions of the model derived based on the above approximation is in good agreement with the results for a binary blend of chemically identical diblock copolymers presented by Lyatskaya et al.[49] (which is based on a more rigorous SST theory) and by Shi et al.[40] (which is based on SCFT). Moreover, in the Supporting Information, we present a comparison between the free energy of a bidisperse flat brush derived based on our approximation with the more accurate theory of Milner and co-workers (Figure 1 of the Supporting Information).[66] In such a context, we demonstrate that the quantitative inaccuracies of our model are less than 20% over a wide range of volume fractions and molecular weight ratios of the two components. These considerations are used to indirectly justify the validity of the above assumption.

In the appendix, we present the general derivation of the elastic free energy of a bidisperse brush containing an arbitrary mixture of chains of kind "1" (with $N_1$ segments each) mixed with chains of kind "2" (with $N_2$ segments each) within the framework of the above assumption for various geometries (cf. eqs A6−A9). Using such free energy expressions, the elastic free energies $F_{II}^{el}$ and $F_{III}^{el}$ corresponding to the regions II and

III can be deduced for the candidate morphologies under consideration.

The enthalpic free energy of mixing in regions II and III, $F^{en}$, can be deduced as:

$$F^{en} = \chi_{BC} \int_{I_1}^{I_2} \mathrm{d}r\ S_D(r)\phi_B(r)\phi_C(r) \tag{13}$$

where the limits $I_1$ and $I_2$ are $H_2^d$ and $H_2^d + H_1^d$ respectively for a BC core configuration, and $H_2^d + H_1^d$ and $H_2^d + H_1^d + H_1^u$ respectively for a A core configuration. In the above equation $S_D(r)$ denotes the surface area element for the $D$ dimensional morphology. To evaluate eq 13, we note that our assumption of proportional stretching of the chains is equivalent to (see eq A5) the following:

$$\phi_A(r) = (1 + \varepsilon_1)^{-1}; \quad \phi_{A_s}(r) = \varepsilon_1(1 + \varepsilon_1)^{-1} \tag{14}$$

$$\phi_B(r) = (1 + \varepsilon_2)^{-1}; \quad \phi_C(r) = \varepsilon_2(1 + \varepsilon_2)^{-1} \tag{15}$$

where $\phi_{A_s}(r)$, $\phi_A(r)$, $\phi_C(r)$, and $\phi_B(r)$ represent the local volume fractions of $A_s$, A, C, and B segments respectively in the regions II and III, and $\varepsilon_1$, $\varepsilon_2$ are constants which are independent of the location within the brush. Moreover, using the constraint of the total number of segments of A, $A_s$, B, and C in regions II and III, we can deduce

$$\varepsilon_1 = \begin{cases} n_s\alpha f_s N/N_1^u & \text{BC core} \\ n_s\alpha f_s/N_1^d & \text{A core} \end{cases} \tag{16}$$

and

$$\varepsilon_2 = \begin{cases} n_s\alpha(1 - f_s)N/N_1^d & \text{BC core} \\ n_s\alpha(1 - f_s)N/N_1^u & \text{A core} \end{cases} \tag{17}$$

Equations 15 and 17, in conjunction with eq 13 enables the evaluation of the free energy $F^{en}$ as a function of $N_1^d$ and $N_1^u$ in various geometries.

To evaluate the interfacial energy of the interface between regions II and III, we require an expression for the interfacial tension between a region which contains A segments and a region which contains a mixture of B and C segments with volume fractions $\phi_B$ (eq 15) and $1 - \phi_B$ respectively. We approximate the $\chi$ between the regions II and III by a simple mixing rule of the form: $\chi_{A|BC} = \phi_B\chi_{AB} + (1 - \phi_B)\chi_{AC}$, and use the expression for the interfacial tension of a polymer blend[80] to evaluate the interfacial tension $\gamma_{I|II}$ between regions I and II:

$$\gamma_{I|II} = b^2\sqrt{\frac{\chi_{A|BC}}{6}} \tag{18}$$

The interfacial energy contribution $F^{int}$ (expressed on a per AB chain basis) is then given as

$$F^{\mathrm{int}} = \gamma_{I|II}\sigma^{-1} \tag{19}$$

Equations 1−13 furnish the complete formulation required for evaluating the free energies of the different morphologies.

**C. Analysis of Phase Diagrams.** The free energy expressions presented in the preceding section are functions of three variables: $\sigma$,$N_1^d$ and $N_1^u$. For specified interaction parameters $\chi_{AB}$, $\chi_{BC}$, and $\chi_{AC}$, and the physical parameters $\alpha$ and $w$, we minimize the free energy of each candidate morphology over the variables $\sigma$, $N_1^d$, and $N_1^u$ to deduce the *optimal* free energy of a morphology. Strictly speaking, characterization of the self-assembly behavior of the system requires analysis of phase coexistences (using Maxwell common tangent analysis) by considering the blend fraction ($w$) dependence of the optimal free energies of the different morphologies.[49] However, the numerical implementation of such two phase coexistences prove extremely cumbersome (cf. Figure 4 for an example), and hence we have restricted ourselves to identifying the equilibrium morphology of the blend system as the structure which possesses the minimum optimal free energy among the different candidate structures.

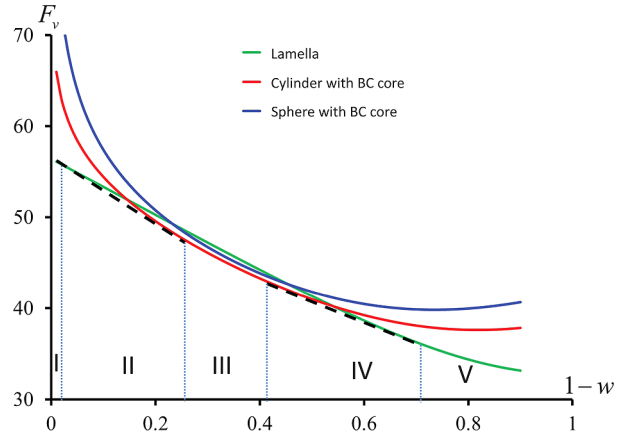


**Figure 4.** Free energy per unit volume $F_v$ of a blend (in units of $k_BTb^{-3}$) of a mixture of lamella forming binary blend of chemically identical diblock copolymers. Parameters correspond to: $f = 0.69$, $f_s = 0.33$, $\alpha = 0.48$, $\chi_{AB}N = 25000$, and $\chi_{BC} = 0$. $w$ represents the weight fraction of the smaller chains (displayed as $1 - w$ to maintain the same orientation of Figure 7 in ref 49.). The dashed black lines denote common tangents of coexistence between lamellar and cylinder morphologies. The regions I, V represent regimes wherein the lamellar morphology is the most stable phase. Regions II and IV represent regimes of coexistence between lamellar and cylindrical phases. Region III represent the regime where the cylindrical morphology is the equilibrium morphology.

For certain sets of parameters, the results of the free energy minimization procedure described above yields lamellar morphologies as the equilibrium phase, but with the brush thickness of the B phase being smaller than the unperturbed radius of gyration of the B portion of the AB chain. In such lamellae, the B portions of the chains are compressed instead of being stretched. This renders SST invalid for such system, but it also means that lamella morphology is highly improbable for given conditions. Indeed, brushes and lamellar phases of compressed chains are known to be susceptible to different kinds of undulational instabilities.[73,81] In the present work, we use our SST model to demarcate (in the physicochemical parameter space) the occurrence of such regimes, and denote them as "unstable lamella" phases in the phase diagram. Unfortunately, the morphology which manifests in such regimes cannot be identified through the model and analysis we have employed in the present work.

A second caveat regarding our model is that our approximation for the elastic free energy of the mixed brush fails when $H_2^d \to 0$ (cf. eqs A8 and A10). As a consequence, our model is unable to access the regime when a small volume fraction of the longer AB chains are mixed with a larger volume fraction of AC chains (i.e., the limit $w \to 1$). Hence, our results for the phase


dx.doi.org/10.1021/ma301402n | Macromolecules 2012, 45, 8729−8742

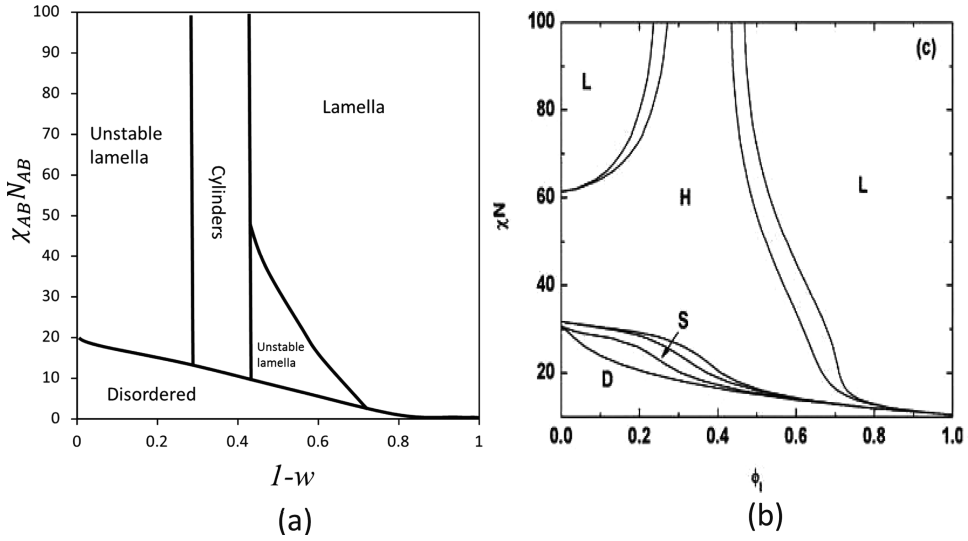


**Figure 5.** Comparison with SCFT phase diagram of ref 40. Parameters correspond to $\alpha = 0.4$, $\chi_{BC} = 0$, $f = 0.5$, and $f_s = 0.35$: (a) results of our SST model; (b) Figure 2b of ref40. $\phi_L$ denotes the volume fraction of the longer copolymers. In our notation, $\phi_L \equiv 1 - w$. L denotes lamellar phase, H denotes cylindrical morphologies, S denotes spheres, and D denotes disordered phase. Reprinted with permission from ref 40.

diagram are expected to be reliable only for regimes such that $w \lesssim 0.8$.

## III. RESULTS

**A. Comparison with the Previous Results for AB + AB Blends.** As discussed in the introduction, a number of earlier theoretical studies have modeled the phase behavior of binary blends of chemically identical diblock copolymers which differ in either their MWs and/or their average compositions. Among the different approaches, the SST based models proposed by Birshtein, Lyatskaya, and Zhulina[46,49,50,67,82] are closest in spirit to the framework adopted in this article. Explicitly, Birshtein and co-workers developed a strong stretching theory of bidisperse brushes for flat and cylindrical geometries. Subsequently, they applied such a theory to the analysis of the phase behavior of a mixture of *chemically identical* copolymers of the form $AB_1 + AB_2$ blends, in which the number of segments in the A blocks of the two copolymers were the same, but the number of segments in $B_1$ and $B_2$ blocks were different. We note that such a system constitutes a specific case of the general theory we presented in section IIB. Explicitly, by appropriate definitions of $f$, $f_s$ and $\alpha$, and by setting $\chi_{BC} = 0$, our model reduces to that of the system considered in ref 49. In this section, we present a brief comparison between the predictions of our model and the results of Lyatskaya et al.[49] Such a comparison is motivated by the fact that the free energy model we developed for bidisperse brushes (Appendix A) is less rigorous than the model proposed by Lyatskaya et al. A comparison of the predictions of our model with the results of Lyatskaya et al.[49] would shed light on the validity of our approximations.

To display a comparison of our results with the predictions of Lyatskaya et al.,[49] we choose a specific result from their article, viz., that in a mixture of two lamella forming copolymers with parameters (in our notation) $f = 0.69$,$f_s = 0.33$ and $\alpha = 0.48$, the following sequence of morphologies were predicted to occur with increasing blending volume fraction $w$: single phase region of lamellae → two-phase coexistence region between lamellae and cylinders → a single phase region of cylinders → a coexistence region between lamellae and cylinders → a single phase region of lamellae. In Figure 4, we display the $w$ dependence for the free energy per volume, $F_v$, from our model for the parameters specified above. One can observe that for both $w \to 0$ and $w \to 1$, the lamellar phase is indeed the most stable morphology. However, it can be seen that at intermediate blending volume fractions, there are regions of coexistence between lamellae and cylinders (indicated schematically through the common tangents). Furthermore, in between the two regions of lamella-cylinder coexistences, we also observe a region wherein cylinder morphologies constitute the equilibrium phase. Overall, the predictions of our SST model are seen to be in very good agreement with the results presented in Lyatskaya et al.[49]

In a series of papers, Shi and co-workers[40,41] and Matsen[42,43] have presented more elaborate SCFT-based numerical calculations of the phase diagrams of bidisperse diblock copolymer blends. In particular, Shi and co-workers[40] have considered the phase behavior of a mixture of binary blends of symmetric diblock copolymers with shorter asymmetric diblock copolymers and studied the resulting phase behavior. Specifically, they found that at low temperatures, the addition of shorter, asymmetric copolymers to the symmetric longer copolymer system leads to a transformation of the lamellar phases to cylindrical phases. In Figure 5, we present a phase diagram based on our model for a comparable set of conditions and compare with the result presented in ref 40. While a quantitative agreement between SCFT calculations and SST cannot be expected for small $\chi N$s, nevertheless we still observe a qualitative correspondence between our results and that of ref 40 (the phase identified as unstable lamella in our model is seen to be predominantly replaced by cylindrical morphologies in SCFT results).

In sum, the above results indicate very good correspondence between the results of our model with both the SST predictions of Lyatskaya et al.[49] and the SCFT predictions of Shi et al.[40] Such an agreement lends support to the approximations used in the development of our SST model and motivates the exploration of the phase behavior of AB + AC blends.

**B. Phase Behavior of AB + AC Blends.** While the theory presented in section IIB is general enough to accommodate a wide variety of AB + AC blends, unfortunately, the parameter space in such systems is too vast to indulge in an exhaustive


dx.doi.org/10.1021/ma301402n | *Macromolecules* 2012, 45, 8729–8742

exploration of all the possible phase behavioral characteristics. Instead of a comprehensive discussion of the parameter space, we focus on parameters which are closely aligned with the experimental conditions which motivated the present theoretical study.[34,35] Explicitly, we set $\chi_{AC} = 5.0\chi_{AB}$ (the experimental conditions are closer to $\chi_{AC}/\chi_{AB} = 6.0-7.0$) for all our calculations. Furthermore, we consider only blends in which the AB and AC copolymers possess identical compositions and therefore set $f = f_s$. Within such a limited parameter space, we present some general results which allows one to understand the extent to which the hydrogen bonding interactions between the B and C segments of the block copolymer can be used as a means to modify the inherent curvatures of the pure component morphologies.

**C. Asymmetric Lamellar Phases from a Mixture of Sphere-Forming Copolymers.** The first set of parameters we consider are representative of the conditions surrounding our first set of experiments.[35] Specifically, we consider the situation of a blend of sphere forming copolymers ($f = f_s = 0.88$) and present the results for the phase diagram (Figure 6a) when $\alpha = 0.2$. For the purpose of constructing the phase diagram we fixed $\chi_{AB}N = 500$ and varied $\chi_{BC}$ in the range indicated. We observe that even for $\chi_{BC} = 0$ (a parametric condition equivalent to a bidisperse blend of chemically identical diblock copolymers), addition of smaller AC copolymers to the AB copolymers transforms the native spherical phases into cylindrical morphologies. In this situation, addition of smaller diblock copolymers to the longer ones leads to a reduction in the stretching energy of the longer copolymers. The latter leads to a concomitant lowering of the spontaneous curvature and the bending moduli of the spherical layers formed by the longer copolymers. As a result, the formation of less curved morphologies such as cylindrical phases becomes favorable.

At larger magnitudes of $\chi_{BC}$, we observe that increasing the volume fractions of AC copolymers transforms the spherical morphologies of AB copolymers to cylinders and eventually to lamellar phases (followed by a transition to cylinders at even larger blending fractions). In section IIA, we suggested that the attractive interactions between the B and C segments (arising from hydrogen bonding interactions) favors a more enhanced mixing of the B and C segments. The latter can be facilitated (within a specified morphology) by a compression of the B segments and a stretching of the C segments, which would lead to a reduction in the period of the equilibrium morphology. Such expectations are seen to be borne out in the results displayed in Figure 6b (and also in the experimental scattering profiles[35]), in which we observe that within a given morphology, the equilibrium periods monotonically decrease within increasing volume fraction of AC copolymers. Alternatively, the mixing between B and C segments can be enhanced by a transformation of the spherical morphologies to a less concave morphology such as cylinders or to the noncurved (lamellar) morphologies. We propose that such driving forces form the basis of the morphological phase transformations observed in Figure 6a.

To support the above hypothesis, we present indirect evidence by demonstrating that the formation of lamellar phase is accompanied by a transition to a complete mixing between the B and C segments. For this purpose, we define a "mixing" parameter $\xi_{BC}$, which quantifies the mixing of B and C segments within a specified morphology. Explicitly,

$$\xi_{BC} = \alpha\frac{1-f}{1-f_s}\epsilon_2 \qquad (20)$$

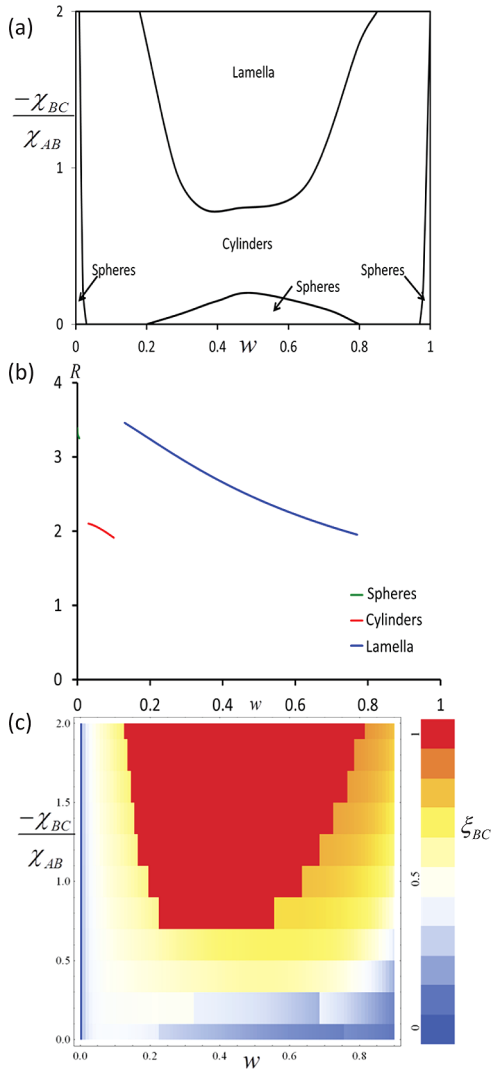


**Figure 6.** (a) Phase diagram for an AB + AC blend as a function of $\chi_{BC}$ (normalized by $\chi_{AB}$) and the weight fraction $w$. The other parameters were $f = f_s = 0.88$, $\alpha = 0.2$, $\chi_{AB}N = 500$. (b) Equilibrium periods of the morphologies as a function of $w$ for $\chi_{BC}/\chi_{AB} = -2.0$. (c) The mixing parameter $\xi_{BC}$ (eq 20) displayed as an intensity plot for the different regions of the phase diagram. The color panel indicated on the right side of the figure quantifies the intensities of $\xi_{BC}$. The jagged shape of the plot is an artifact of the resolution with which we computed $\xi_{BC}$.

where $\epsilon_2$, defined in eq 17, represents the intermixing between B and C segments in a given morphology. The mixing parameter $\xi_{BC}$ defined above is normalized such that $\xi_{BC} \leq 1$, in which the limit $\xi_{BC} = 1$ represents the case where $B$ and $C$ subchains are fully intermixed such that the sizes of $B$ and $C$ subchains are identical. The results for $\xi_{BC}$ in the different regions of the phase diagram are displayed in Figure 6c. It can be seen that increasing $|\chi_{BC}|$ leads to an increase in $\xi_{BC}$—a trend which is consistent with the enhanced favorable interactions between B and C segments. Moreover, from the displayed values of $\xi_{BC}$, it can be seen that in the lamellar phases $\xi_{BC} \simeq 1$, which corresponds to a complete overlap between the B and C segments. In contrast, it can be seen that in the cylindrical phases, $\xi_{BC} \lesssim 0.5$, which corresponds to only a partial intermixing between B and C segments.

The lamellar morphologies which are generated in the above mixtures are of significant interest since the thickness of the


dx.doi.org/10.1021/ma301402n | Macromolecules 2012, 45, 8729–8742

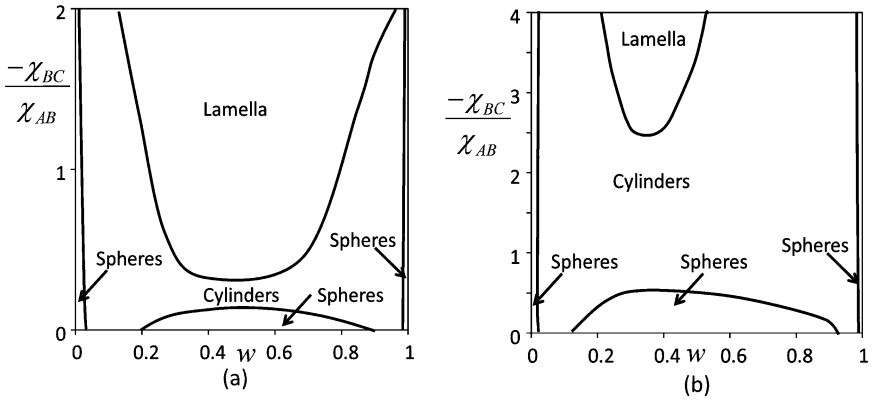


**Figure 7.** (a) Phase diagram for an AB + AC blend as a function of $\chi_{BC}$ (normalized by $\chi_{AB}$) and the weight fraction $w$. The other parameters were $f = f_s = 0.88$, $\alpha = 0.2$, $\chi_{AB}N = 100$. (b) Phase diagram for an AB + AC blend as a function of $\chi_{BC}$ (normalized by $\chi_{AB}$) and the weight fraction $w$. The other parameters were $f = f_s = 0.93$, $\alpha = 0.2$, and $\chi_{AB}N = 100$.

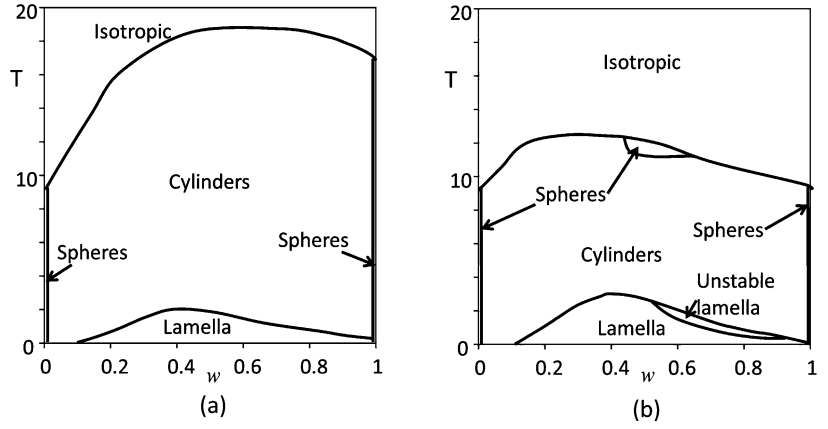


**Figure 8.** Phase diagram of a blend of AB + AC copolymers as a function of temperature and AC volume fraction $w$. The parameters correspond to $f = f_s = 0.88$, $\chi_{AB}N = 250T^{-1}$, $\chi_{BC} = -2\chi_{AB}$. Key: (a) $\alpha = 0.2$; (b) $\alpha = 0.4$.

A zones in such phases are much larger than the thickness of the B + C zones. Explicitly, we have

$$\frac{L_{AA_s}}{L_{BC}} = \frac{wf + (1-w)f_s}{w(1-f) + (1-w)(1-f_s)} \tag{21}$$

where $L_{AAs}$ and $L_{BC}$ are the thicknesses of $AA_s$ and BC portions of lamellae. For instance, for the parametric conditions considered in Figure 6, we have $L_{AA_s}/L_{BC} \simeq 7$. As discussed in the introduction to this article, strategies to realize such asymmetric lamellar phases are quite limited within the context of flexible block copolymers. The idea explored in this article (as a complement to our experimental work) demonstrates a versatile strategy to realize such a goal in which the asymmetry of the lamellae thicknesses can be tuned simply by changing $f$, $f_s$ and $w$ (for $f = f_s$, $w$ does not influence the thickness ratios). Furthermore, in our recent article[35] we showed that the idea explored in this article can be successfully transferred to thin film situations with the asymmetric lamellar microdomains aligned perpendicular to the substrate. The latter demonstration suggests significant potential for applications in the context of next-generation soft lithography techniques.

While the parameters used in Figure 6 were chosen specifically to mimic our experimental conditions, in light of the potential for applications of such asymmetric lamellae, it is of interest to explore some of the parametric dependencies of the phase behavior depicted in Figure 6. Among the different parameters which modulate the driving forces for the curvature changes, it is evident that a critical parameter is the strength of the hydrogen bonding interactions, $\chi_{BC}$. Indeed, it is clear from Figure 6, that $\chi_{BC}$ needs to be large enough (in magnitude) for achieving lamellar phases. On the other hand, the elastic constants and the ease with which the morphologies can transform from spherical to cylindrical and lamellar phases are expected to be related directly to the strength of repulsive interactions $\chi_{AB}$.[83] Hence, we expect that the transformation to lamellar phases would become more favorable in systems with smaller $\chi_{AB}$. In Figure 7a, we validate such speculations by presenting the results for phase diagram with $\chi_{AB}N = 100$. Consistent with our reasoning above, we observe that the region of lamellar phase becomes considerably expanded relative to Figure 6a. These results suggest that lamellar phases may be achieved with a much lower strength of associative interactions if the corresponding $\chi_{AB}$ is also smaller.

Another question of significant practical interest is whether there is a limit to the lamellar asymmetries which can be achieved. To address this issue, we probed the phase behavior of the system with $f = f_s = 0.93$ (which would correspond to a asymmetry of 13.3 in the widths of the lamellae) and $\chi_{AB} = 100.0$. From the results depicted in Figure 7b (and by comparison to the results of Figure 7a), we observe that the lamellar phase is considerably shrunken for larger $f$. Moreover, significantly stronger attractive interactions between B and C segments are seen to be necessary to achieve the lamellar phases.


dx.doi.org/10.1021/ma301402n | Macromolecules 2012, 45, 8729–8742

These results can be understood by noting that copolymers possessing significant compositional asymmetry (e.g., $f \gtrsim 0.9$) involve much stronger bending forces and spontaneous curvature effects which render the A component as the matrix phase.[77] Hence, much stronger attractive interactions between B and C segments are necessitated to overcome such forces and transform the spherical morphologies to lamella phases.

Another parameter which influences the driving force for curvature modifications is the molecular weight (MW) disparity $\alpha$ of the chains. Indeed, for larger $\alpha$ (equivalent to a larger C subchain), significant intermixing of B and C segments can occur without incurring a concomitant stretching of the C chains or compression of the B chains. As a consequence, the forces underlying the transformations to nonconcave BC structures become weaker. In Figures 8a and b, we compare the results for $\alpha = 0.2$ and $\alpha = 0.4$ and demonstrate that such expectations are indeed borne out. Explicitly, for the case of larger $\alpha$, we observe that we require lower temperatures (equivalent to stronger B−C interactions) for the transition to the lamellar phases.

Interestingly, we observe that while smaller $\alpha$ does facilitate a transition to the lamellar phases at higher temperatures, nontrivial behavior may arise in such situations due to the conformational changes required of the B chains to accommodate the morphological behaviors. Indeed, as discussed earlier, at large volume fractions of AC chains, the B chains may be forced to compress to a size less than their unperturbed size. We suggested that the latter occurrence usually signals that the lamellar phase may be sensitive to instabilities. In Figure 8a, we observe such a region of instability appears at larger $w$s. As a consequence, copolymer blends with a smaller $\alpha$ may actually have a smaller window of blending fractions $w$ over which stable lamella phase can be achieved. Consistent with such expectations, in our experimental results,[35] we observed that the lamella phase could be stabilized even up to $w = 0.9$ for the case of $\alpha = 0.4$. In contrast, for $\alpha = 0.2$ we could not achieve stable lamellar phases beyond $w \simeq 0.65$.

**D. Blend of Lamella Forming Symmetric Copolymers.** In this section, we consider parameters related to our second set of experiments in which a mixture of lamella forming block copolymers were used to create *symmetric* cylindrical and spherical morphologies.[34] We first present results which demonstrate that our model is able to capture the trends observed in our experiments. The physical ideas and driving forces underlying the morphological transitions are identical to those elaborated in the preceding section. Hence, in this section, we restrict our discussion to only a few other results which mainly relate to the extrapolation of the general concept to other parametric conditions.

To recall, our second set of experiments considered a mixture of two symmetric copolymers with $f = f_s = 0.5$, and two different MW ratios corresponding to $\alpha = 0.48$ and $\alpha = 0.07$. When $\alpha = 0.48$, addition of AC copolymers transformed the lamellar morphologies of the AB copolymers to a hexagonally arranged cylindrical phase. In contrast, for the case of $\alpha = 0.07$, a sequence of transformations were observed in which lamellae were first transformed to cylinders and subsequently to spherical morphologies with increasing volume fraction of AC copolymers.

In Figure 9a, we present the results for the case of $\alpha = 0.48$. We observe that within the SST model, our phase diagram indicates the presence of a large region corresponding to "unstable lamella." While a portion of this region may indeed correspond to the experimentally observed cylindrical morphologies, it is not possible to unequivocally ascribe a morphology to such parametric conditions without a much more involved analysis. To complement the above result, we explored the phase behavior

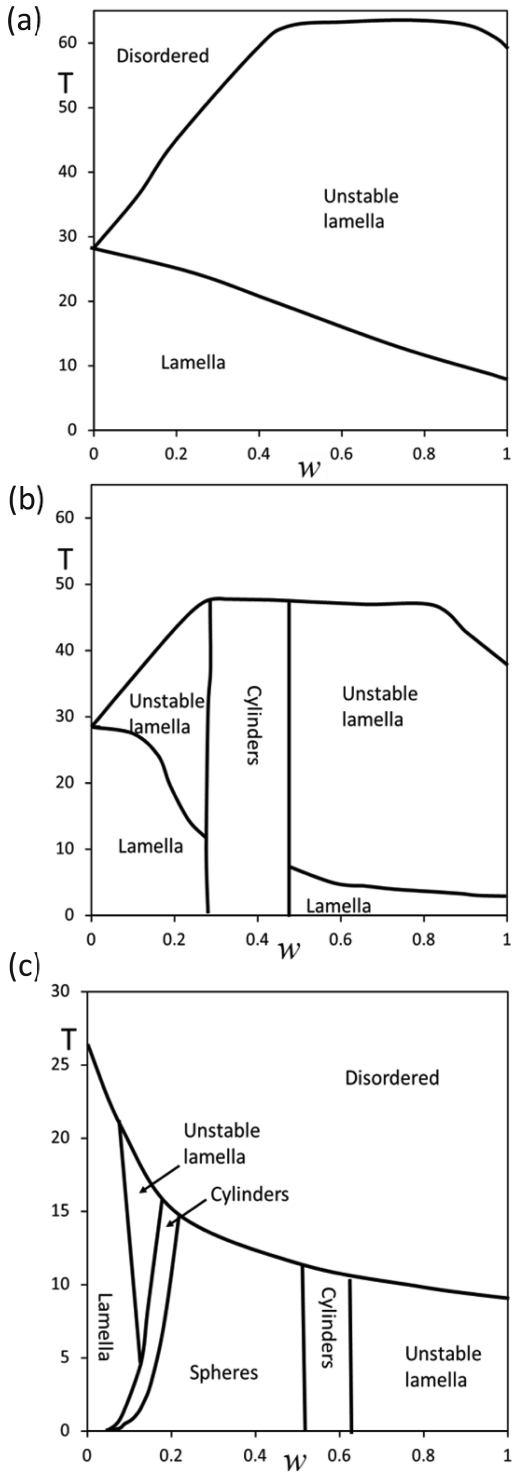


**Figure 9.** Phase diagram of a blend of AB + AC copolymers as a function of temperature and AC volume fraction $w$. The parameters correspond to $f = f_s = 0.5$, $\chi_{AB}N = 250T^{-1}$, $\chi_{BC} = -2\chi_{AB}$. Key: (a) $\alpha = 0.48$; (b) $\alpha = 0.35$; (c) $\alpha = 0.07$.

of a system with a smaller $\alpha$ corresponding to $\alpha = 0.35$ (Figure 9b). In such a system, it is seen that our model indeed predicts a sequence of morphological transitions which matches our experimental observations. Finally, in Figure 9c, we present results corresponding to $\alpha = 0.07$. For such a case, we again observe a sequence of phase transitions which matches qualitatively with the trends noted in the experiments.


dx.doi.org/10.1021/ma301402n | Macromolecules 2012, 45, 8729−8742

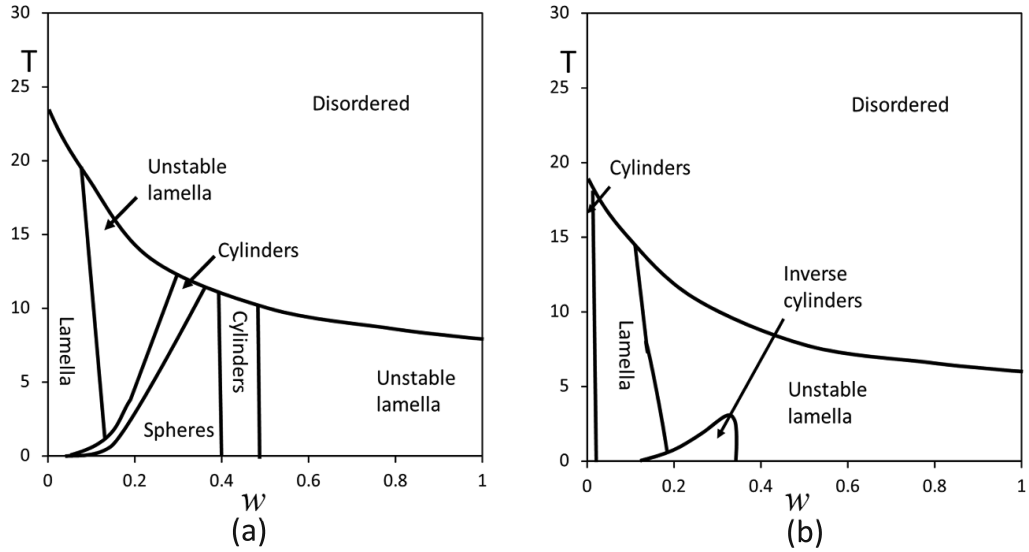


**Figure 10.** Phase diagram of a blend of AB + AC copolymers as a function of temperature and AC volume fraction $w$. The parameters correspond to $\alpha = 0.07$, $\chi_{AB}N = 250T^{-1}$, and $\chi_{BC} = -2\chi_{AB}$. Key: (a) $f = f_s = 0.65$; (b) $f = f_s = 0.75$.

The mechanistic driving forces underlying the above morphological transformations are essentially the same as those discussed in the preceding section. Explicitly, the attractive interactions between the B and C segments causes a spontaneous bending force of the A−(B−C) interface toward the A region. If such bending forces are strong enough, the lamella phase can be transformed into cylindrical or spherical morphologies with B and C segments constituting the matrix phase. The theoretical results presented in Figure 9c and the corresponding experimental observations indicate that the driving force for such curvature modifications are significantly stronger when shorter AC chains are added to the AB copolymers. The origins of such behavior was rationalized in the previous section in the context of Figure 8.

In the curved phases formed in the above-considered systems, the volume of the A phase, denoted $V_{A+A_s}$, and the volume of the B+C phases, denoted $V_{B+C}$, are related through

$$\frac{V_{A+A_s}}{V_{B+C}} = \frac{wf + (1-w)f_s}{w(1-f) + (1-w)(1-f_s)} \tag{22}$$

For $f = f_s$, we have

$$\frac{V_{A+A_s}}{V_{B+C}} = \frac{f}{1-f} \tag{23}$$

From eq 23, we deduce that the spherical and cylindrical phases observed in Figure 9 possess an interesting property that the volume of the internal phase (consisting of A segments) is identical to the volume of the external phase. As mentioned in the introduction, curved phases with such high internal volume could be of potential interest in separation and catalytic applications. Motivated by such considerations, we probe the limits to which the above concept can extended. Specifically, we query whether internal spherical phases in which the volume of the core is *larger* than the matrix can be achieved. Also, we probe whether a cylindrical phase with a matrix of A segments can be made to form an "inverted cylindrical phase" with A segments in the core region.

It is evident that the answers to the above questions would depend on the different interaction parameters and compositions. For illustrative purposes, we fixed all the interaction parameters to their values corresponding to Figure 9. Subsequently, we explored a few other values for $f$ (while maintaining it to be equal to $f_s$) and fixed $\alpha = 0.07$. In Figure 10a, we display the results for the case of a mixture of AB + AC block copolymers with $f = f_s = 0.65$. This corresponds to a situation in which the native AB and AC copolymers form lamellar phases. However, it is seen that by appropriate blending conditions and temperatures, spherical phases (possessing an internal volume which is 65% the matrix volume) can be achieved. When we explored another case of lamellar forming block copolymers corresponding to $f = f_s = 0.7$ (results not displayed), the spherical morphologies were no longer a possible equilibrium structure. These considerations suggest that for the present set of parameters, the sphere phases perist up to $f = f_s \simeq 0.65-0.7$. In Figure 10b, we display the results for the $f = f_s = 0.75$. In this case, the native block copolymers form cylinder phases (with A segments constituting the matrix). We observe that even for this significantly A rich block copolymers, we are able to form an inverted cylinder phase (with A segments constituting the core) at appropriate temperature and blending fractions. Together the results presented in Figures 10a and b suggests that the use of hydrogen bonding intereactions provides a versatile strategy to modulate the curvature of the phases and create morphologies which may not be achievable by other means.

## IV. SUMMARY

In this article, we presented a strong stretching theory for microphase segregation of AB + AC block copolymer blends in which the B and C segments possess strong associative interactions. The main outcome of our theory is the demonstration that in the microdomain morphologies, the attraction between the longer B chains and the shorter C chains may cause a bending force toward the A layers. Such bending force, if strong enough, may cause transitions from symmetric lamella phases and cylindrical phases (with A the majority component) to cylindrical or spherical phases with B−C phase becoming the "matrix" component. In a blend of asymmetric copolymers, similar interactions can drive a transition from a spherical phase to a cylinder phase or to an asymmetric lamella phase.

Our model encapsulated the underlying physics within simple approximations and delineated the parametric dependence of


dx.doi.org/10.1021/ma301402n | *Macromolecules* 2012, 45, 8729−8742

the phase transformations. These results were shown to be in qualitative agreement with experiments. Specifically, we showed that the smaller AC copolymers and/or stronger BC interactions promote the above curvature transformations. By appropriate choice of parameters, we showed that significantly asymmetric lamellae can be achieved. In a similar manner, high volume cylindrical and spherical phases with the interior of the cylinder and spheres occupying of the order 65%−75% of the total volume can also be achieved.

The present work can be extended in a number of directions. For instance, all our results assumed that our AB + AC blends were such that the average compositions of the AB and AC copolymers were the same ($f = f_s$). Relaxing this assumption may lead to significantly richer morphological phase diagrams. Also, strong segregation theory, while useful in its analytical simplicity and the ability to capture the qualitative aspects of phase transitions, is known to be quantitatively inaccurate except at very high degrees of segregation.[11,84] A natural complement to this work would be to probe the quantitative aspects of the phase transitions using self-consistent field theory.[37,85] Finally, as mentioned in the text, our model is general enough to accommodate the behavior of AB + CD blends with associative interactions between the A−D and B−C pairs. The phase behavior of such blends would also be an interesting direction for future study.

## APPENDIX A: ELASTIC FREE ENERGIES OF BIDISPERSE BRUSHES

In this section we present our model for the elastic free energy of the bidisperse brush present in the mixed regions II and III of Figure 3. As mentioned in the main article text, our model for the mixed portion of the brush is based on the DeGennes−Alexander approximation (DGA) for flat brushes and invokes that the free end distribution of the chains is a delta function at the appropriate height. Moreover, we assume that the local stretching of the two kinds of chains which constitute the brush are proportional to each other, and that the proportionality between the local stretching of the chains is independent of the location in the plane normal to the grafting surface.

We consider a bidisperse brush made of chains we denote generally as "1" and "2." The number of segments in "1" and "2" are denoted as $N_1$ and $N_2$ respectively. The grafting density of chains of type "1" is denoted as $\sigma$. We use the symbol $n_s$ to denote the number of chains of type "2" per chain of type "1." The starting point for our calculation of the elastic energy contribution of the bidisperse brush is the formula for the stretching free energy $\delta F^{el}$ of a polymer chain of $\Delta n$ segments and end-to-end distance $\Delta x$:[63,64]

$$\delta F^{el} = \frac{3}{2b^2}\frac{(\Delta x)^2}{\Delta n} = \frac{3}{2b^2}E(x)\Delta x \tag{A1}$$

where $E(x) = \Delta x/\Delta n$ represents the local stretching of a polymer chain.[63] The elastic free energy of a heterogeneously stretched chain in a grafted layer extending from $I_1$ to $I_2$ is then given as

$$F^{el} = \frac{3}{2b^2}\int_{I_1}^{I_2} \mathrm{d}r\; S_D(r)E(r) \tag{A2}$$

where $S_d(r)$ denotes the surface area element for the $D$ dimensional morphology. In the above expression eq A2, we have made use of the deGennes−Alexander approximation by setting the free end distribution of the short chains corresponds to a delta function at the edge of the brush ($I_2$ in the above notation).[78,79] The local density of the segments $\phi(r)$ is given by[63,64]

$$\phi(r) = \frac{b^3\sigma\left(1 \pm \frac{r}{R}\right)^{D-1}}{E(r)} \tag{A3}$$

where the "+" applies for convex brushes and the "−" sign for concave brushes.

As mentioned in the article text, we have assumed that the bidisperse brush is such that the local stretching of the two components are proportional to each other, with the proportionality constant independent of the location inside the brush. Using eq A3, it can be seen that such an assumption is equivalent to a relationship of the form

$$\phi_2(r) = \varepsilon\phi_1(r) \tag{A4}$$

where $\phi_1(r)$ and $\phi_2(r)$ denote the local volume fractions of segments of types 1 and 2 respectively. In conjunction with the incompressibility constraint, $\phi_1(r) + \phi_2(r) = 1$, eq A4 yields explicit expressions for $\phi_1(r)$ and $\phi_2(r)$:

$$\phi_1(r) = (1 + \varepsilon)^{-1}; \quad \phi_2(r) = \varepsilon(1 + \varepsilon)^{-1} \tag{A5}$$

Substitution of eq A5 in eq A3, allows us to deduce the local stretching of the chains $E(r)$. Use of the latter in eq A2 furnishes the required elastic stretching energy contributions in different geometries. The final expressions elastic free energies are listed below:

(i) For a flat brush of height $H$:

$$F^{el} = \frac{3Hb(N_1 + N_2)\sigma(N_2{n_s}^2 + N_1)}{2N_1N_2} \tag{A6}$$

(ii) For a convex cylindrical brush of height $H$ grafted on a surface of radius $R$:

$$F^{el} = \frac{3bR\sigma(N_1 + N_2)(N_2{n_s}^2 + N_1)\log\left(1 + \frac{H}{R}\right)}{2N_1N_2} \tag{A7}$$

(iii) For a concave cylindrical brush of height $H$ grafted on a surface of radius $R$:

$$F^{el} = \frac{3bR\sigma(N_1 + N_2)(N_2{n_s}^2 + N_1)\log\left(1 - \frac{H}{R}\right)}{2N_1N_2} \tag{A8}$$

(iv) For a convex spherical brush of height $H$ grafted on a surface of radius $R$:

$$F^{el} = \frac{3bR\sigma(N_1 + N_2)(N_2{n_s}^2 + N_1)}{2N_1N_2\left(1 + \frac{R}{H}\right)} \tag{A9}$$

(v) For a concave spherical brush of height $H$ grafted on a surface of radius $R$:

$$F^{el} = \frac{3bR\sigma(N_1 + N_2)(N_2{n_s}^2 + N_1)}{2N_1N_2\left(\frac{R}{H} - 1\right)} \tag{A10}$$

## ASSOCIATED CONTENT

### Supporting Information

Comparisons of the free energies of a bidisperse brush to earlier predictions. This material is available free of charge via the Internet at http://pubs.acs.org.

## AUTHOR INFORMATION


### Corresponding Author

*E-mail: venkat@che.utexas.edu.


### Notes

The authors declare no competing financial interest.

## ACKNOWLEDGMENTS

This work was supported partially by a grant from Robert A. Welch Foundation (Grant F1599), the US Army Research Office under Grant W911NF-10-10346, and the National Science Foundation (DMR 1005739). J.K.K. acknowledges support from the National Creative Research Initiative Program supported by the National Research Foundation (NRF) of KOREA.

## REFERENCES


(1) Park, C.; Yoon, J.; Thomas, E. L. *Polymer* **2003**, *44*, 6725−6760.
(2) Hamley, I. W. *Angew. Chem., Int. Ed.* **2003**, *42*, 1692−1712.
(3) Cheng, J. Y.; Ross, C. A.; Smith, H. I.; Thomas, E. L. *Adv. Mater.* **2006**, *18*, 2505−2521.
(4) Olson, D. A.; Chen, L.; Hillmyer, M. A. *Chem. Mater.* **2008**, *20*, 869−890.
(5) Olsen, B. D.; Shah, M.; Ganesan, V.; Segalman, R. A. *Macromolecules* **2008**, *41*, 6809−6817.
(6) Kim, J. K.; Lee, J. I.; Lee, D. H. *Macromol. Res.* **2008**, *16*, 267−292.
(7) Bang, J.; Jeong, U.; Ryu, D. Y.; Russell, T. P.; Hawker, C. J. *Adv. Mater.* **2009**, *21*, 4769−4792.
(8) Gomez, E. D.; Panday, A.; Feng, E. H.; Chen, V.; Stone, G. M.; Minor, A. M.; Kisielowski, C.; Downing, K. H.; Borodin, O.; Smith, G. D.; Balsara, N. P. *Nano Lett.* **2009**, *9*, 1212−1216.
(9) Kim, J. K.; Yang, S. Y.; Lee, Y.; Kim, Y. *Prog. Polym. Sci.* **2010**, *35*, 1325−1349.
(10) Jha, A. K.; Chen, L.; Offeman, R. D.; Balsara, N. P. *J. Membr. Sci.* **2011**, *373*, 112−120.
(11) Matsen, M. W.; Bates, F. S. *Macromolecules* **1996**, *29*, 1091−1098.
(12) Bates, F. S.; Fredrickson, G. H. *Phys. Today* **1999**, *52*, 32−38.
(13) Cochran, E. W.; Garcia-Cervera, C. J.; Fredrickson, G. H. *Macromolecules* **2006**, *39*, 2449−2451.
(14) Yang, S. Y.; Ryu, I.; Kim, H. Y.; Kim, J. K.; Jang, S. K.; Russell, T. P. *Adv. Mater.* **2006**, *18*, 709−+.
(15) Yang, S. Y.; Park, J.; Yoon, J.; Ree, M.; Jang, S. K.; Kim, J. K. *Adv. Funct. Mater.* **2008**, *18*, 1371−1377.
(16) Jo, A.; Joo, W.; Jin, W. H.; Nam, H.; Kim, J. K. *Nature Nanotechnol.* **2009**, *4*, 727−731.
(17) Beardsley, T. M.; Matsen, M. W. *Eur. Phys. J. E* **2010**, *32*, 255−264.
(18) Matsen, M. W. *J. Phys.: Condens. Matter* **2002**, *14*, R21−R47.
(19) Hashimoto, T.; Kimshima, K.; Hasegawa, H. *Macromolecules* **1991**, *24*, 5704−5712.
(20) Hashimoto, T.; Koizumi, S.; Hasegawa. *Macromolecules* **1994**, *27*, 1562−1570.
(21) Koizumi, S.; Hasegawa, H.; Hashimoto, T. *Macromolecules* **1994**, *27*, 4371−4381.
(22) Yamaguchi, D.; Bodycomb, J.; Koizumi, S.; Hashimoto, T. *Macromolecules* **1999**, *32*, 5884−5894.
(23) Yamaguchi, D.; Shiratake, S.; Hashimoto, T. *Macromolecules* **2000**, *33*, 8258−8268.
(24) Yamaguchi, D.; Takenaka, M.; Hasegawa, H.; Hashimoto, T. *Macromolecules* **2001**, *34*, 1707−1719.
(25) Yamaguchi, D.; Hasegawa, H.; Hashimoto, T. *Macromolecules* **2001**, *34*, 6506−6518.
(26) Court, F.; Yamaguchi, D.; Hashimoto, T. *Macromolecules* **2006**, *39*, 2596−2605.
(27) Court, F.; Yamaguchi, D.; Hashimoto, T. *Macromolecules* **2008**, *41*, 4828−4837.
(28) Court, F.; Hashimoto, T. *Macromolecules* **2001**, *34*, 2536−2545.
(29) Court, F.; Hashimoto, T. *Macromolecules* **2002**, *35*, 2566−2575.
(30) Papadakis, C. M.; Mortensen, K.; Posselt, D. *Eur. Phys. J. B* **1998**, *4*, 325−332.
(31) Spontak, R. J.; Fung, J. C.; Braunfeld, M. B.; Sedat, J. W.; Agard, D. A.; Kane, L.; Smith, S. D.; Satkowski, M. M.; Ashraf, A.; Hajduk, D. A.; Gruner, S. M. *Macromolecules* **1996**, *29*, 4494−4507.
(32) Kane, L.; Satkowski, M. M.; Smith, S. D.; Spontak, R. J. *Macromolecules* **1996**, *29*, 8862−8870.
(33) Zhao, J.; Majumdar, B.; Schulz, M. F.; Bates, F. S.; Almdal, K.; Mortensen, K.; Hajduk, D. A.; Gruner, S. M. *Macromolecules* **1996**, *29*, 1204−1215.
(34) Han, S. H.; Kim, J. K.; Pryamitsyn, V.; Ganesan, V. *Macromolecules* **2011**, *44*, 4970−4976.
(35) Han, S. H.; Pryamitsyn, V.; Bae, D.; Ganesan, V.; Kim, J. K. *ACS Nano* **2012**, *6*, 7966−7972.
(36) Fredrickson, G. H.; Ganesan, V.; Drolet, F. *Macromolecules* **2002**, *35*, 16−39.
(37) Fredrickson, G. *The Equilibrium Theory of Inhomogeneous Polymers*; Oxford University Press: Oxford, U.K.,2005.
(38) Shi, A. C.; Noolandi, J. *Macromolecules* **1995**, *28*, 3103−3109.
(39) Lin, E. K.; Gast, A. P.; Shi, A. C.; Noolandi, J.; Smith, S. D. *Macromolecules* **1996**, *29*, 5920−5925.
(40) Wu, Z.; Li, B.; Jin, Q.; Ding, D.; Shi, A.-C. *J. Phys. Chem. B* **2010**, *114*, 15789−15798.
(41) Wu, Z.; Li, B.; Jin, Q.; Ding, D.; Shi, A.-C. *Macromolecules* **2011**, *44*, 1680−1694.
(42) Matsen, M. W. *J. Chem. Phys.* **1995**, *103*, 3268−3271.
(43) Matsen, M. W.; Bates, F. S. *Macromolecules* **1995**, *28*, 7298−7300.
(44) Spontak, R. J. *Macromolecules* **1994**, *27*, 6363−6370.
(45) Spiro, J. G.; Illy, N.; Winnik, M. A.; Vavasour, J. D.; Whitmore, M. D. *Macromolecules* **2012**, *45*, 4289−4294.
(46) Birshtein, T. M.; Liatskaya, Y. V.; Zhulina, E. B. *Polymer* **1990**, *31*, 2185−2196.
(47) Zhulina, E. B.; Birshtein, T. M. *Polymer* **1991**, *32*, 1299−1308.
(48) Zhulina, E. B.; Lyatskaya, Y. V.; Birshtein, T. M. *Polymer* **1992**, *33*, 332−342.
(49) Lyatskaya, J.; Zhulina, E.; Birshtein, T. *Polymer* **1992**, *33*, 343−351.
(50) Birshtein, T. M.; Lyatskaya, Y. V.; Zhulina, E. B. *Polymer* **1992**, *33*, 2750−2756.
(51) Vilesov, A. D.; Floudas, G.; Pakula, T.; Melenevskaya, E. Y.; Birshtein, T. M.; Lyatskaya, Y. V. *Macromol. Chem. Phys.* **1994**, *195*, 2317−2326.
(52) Asari, T.; Matsuo, S.; Takano, A.; Matsushita, Y. *Macromolecules* **2005**, *38*, 8811−8815.
(53) Asari, T.; Matsuo, S.; Takano, A.; Matsushita, Y. *Polym. J.* **2006**, *38*, 258−263.
(54) Tang, C. B.; Hur, S. M.; Stahl, B. C.; Sivanandan, K.; Dimitriou, M.; Pressly, E.; Fredrickson, G. H.; Kramer, E. J.; Hawker, C. J. *Macromolecules* **2010**, *43*, 2880−2889.
(55) Salim, N. V.; Guo, Q. P. *J. Phys. Chem. B* **2011**, *115*, 9528−9536.
(56) Zhu, K. J.; Chen, S. F.; Ho, T.; Pearce, E. M.; Kwei, T. K. *Macromolecules* **1990**, *23*, 150−154.
(57) van Ekenstein, G. O. R. A.; Meyboom, R.; ten Brinke, G.; Ikkala, O. *Macromolecules* **2000**, *33*, 3752−3756.
(58) Zha, W. B.; Han, C. D.; Lee, D. H.; Han, S. H.; Kim, J. K.; Kang, J. H.; Park, C. *Macromolecules* **2007**, *40*, 2109−2119.
(59) Han, S. H.; Lee, D. H.; Kim, J. K. *Macromolecules* **2007**, *40*, 7416−7419.
(60) Dobrosielska, K.; Wakao, S.; Takano, A.; Matsushita, Y. *Macromolecules* **2008**, *41*, 7695−7698.
(61) Dobrosielska, K.; Wakao, S.; Suzuki, J.; Noda, K.; Takano, A.; Matsushita, Y. *Macromolecules* **2009**, *42*, 7098−7102.
(62) Shi, A. C.; Noolandi, J. *Macromolecules* **1994**, *27*, 2936−2944.
(63) Semenov, A. N. *Sov. Phys. JETP* **1985**, *61*, 733−742.
(64) Milner, S. T.; Witten, T. A.; Cates, M. E. *Macromolecules* **1988**, *21*, 2610−2619.

(65) Milner, S. T. *J. Chem. Soc., Faraday Trans.* **1990**, *86*, 1349−1353.
(66) Milner, S. T.; Witten, T. A.; Cates, M. E. *Macromolecules* **1989**, *22*, 853−861.
(67) Zhulina, E. B.; Borisov, O. V.; Pryamitsyn, V. A.; Birshtein, T. M. *Macromolecules* **1991**, *24*, 140−149.
(68) Likhtman, A. E.; Semenov, A. N. *Macromolecules* **1994**, *27*, 3103−3106.
(69) Olmsted, P. D.; Milner, S. T. *Macromolecules* **1998**, *31*, 4011−4022.
(70) Phan, S.; Fredrickson, G. H. *Macromolecules* **1998**, *31*, 59−63.
(71) Pryamitsyn, V.; Ganesan, V. *J. Chem. Phys.* **2004**, *120*, 5824−5838.
(72) Shah, M.; Pryarnitsyn, V.; Ganesan, V. *Macromolecules* **2008**, *41*, 218−229.
(73) Pryamitsyn, V.; Ganesan, V. *Macromolecules* **2006**, *39*, 8499−8510.
(74) Ganesan, V.; Ellison, C. J.; Pryamitsyn, V. *Soft Matter* **2010**, *6*, 4010−4025.
(75) Lefevre, N.; Daoulas, K. C.; Mueller, M.; Gohy, J.-F.; Fustin, C.-A. *Macromolecules* **2010**, *43*, 7734−7743.
(76) Nakamura, I.; Shi, A.-C. *J. Phys. Chem. B* **2011**, *115*, 2783−2790.
(77) Milner, S. T.; Witten, T. A. *J. Phys.* **1988**, *49*, 1951−1962.
(78) Alexander, S. *J. Phys.* **1977**, *38*, 983−987.
(79) DeGennes, P. G. *Macromolecules* **1980**, *13*, 1069−1075.
(80) Helfand, E.; Tagami, Y. *J. Polym. Sci., Part B: Polym. Lett.* **1971**, *9*, 741−&.
(81) Pryamitsyn, V.; Ganesan, V. *J. Chem. Phys.* **2004**, *120*, 5824−5838.
(82) Zhulina, E.; Halperin, A. *Macromolecules* **1992**, *25*, 5730.
(83) Matsen, M. W. *J. Chem. Phys.* **1999**, *110*, 4658−4667.
(84) Matsen, M. W. *J. Chem. Phys.* **2001**, *114*, 10528−10530.
(85) Matsen, M.; Schick, M. *Macromolecules* **1994**, *27*, 187.